Development of multifunctional nano/ultrafiltration membrane based on a chitosan thin film on alginate electrospun nanofibres

T.C. Mokhena[1,2], A.S. Luyt[3]*

[1] *CSIR Materials Science and Manufacturing, Polymers and Composites, Port Elizabeth, South Africa.*

[2] *Department of Chemistry, University of the Free State (Qwaqwa Campus), Phuthaditjhaba, South Africa*

[3] *Center for Advanced Materials, Qatar University, Doha, Qatar*

Abstract

The aim of this study was to develop a high flux three-tier composite membrane composed of a coating layer based on chitosan and chitosan with silver nanoparticles, electrospun alginate nanofibres as a midlayer and nonwoven as a mechanical support substrate. The nanofibres were prepared by electrospinning of alginate with the aid of synthetic electrospinnable polyethylene oxide (PEO), and ionically crosslinked with calcium chloride followed by chemical crosslinking using glutaraldehyde. The silver nanoparticles were synthesized using a chitosan solution and thermal treatment. The silver nanoparticles were found to be well dispersed on the coating layer, which improved the antibacterial activity of the membrane against both gram negative and gram positive bacteria. The chitosan and silver nanoparticles containing chitosan coated membrane displayed similar flux and a high rejection of nanoparticles (> 98%) and oil (> 93%). Both membranes showed a higher flux rate and oil rejection than the commercial membrane. The presence of silver nanoparticles improved the dye rejection, reaching more than 95% rejection throughout the five filtration cycles test. These observations show that the incorporation of silver nanoparticles can enhance the antibacterial activity of the membrane with a promising potential in the field of dye removal and oil separation.

Keywords: Electrospun alginate; Chitosan; Silver nanoparticles; Filtration membrane; Water purification

* Corresponding author (aluyt@qu.edu.qa)

1. Introduction

An ideal filtration membrane must have both high selectivity and flux, long service life and low energy consumption [1]. Efforts for achieving this goal are leading to the replacement of traditional filtration membranes with new advanced thin-film composite (TFC) membranes [2,3]. TFC membranes are composed of two or more different layers, i) a top thin selective barrier, ii) a porous mid-layer, and iii) a bottom mechanical support layer. These conventional TFC membranes are typically made from synthetic polymers such as polyethersulphone, polyacrylonitrile, polyimide, aliphatic polyamide, poly(vinyl fluoride) and polyetherether ketone by a phase immersion process [1]. This process leads to some limitations such as low flux and high fouling due to an asymmetrical pore structure and a relatively broad pore size distribution [4,5]. Nowadays much research is being devoted to the production of nanofibre-based TFC membranes, especially from electrospinning [2,4]. It was demonstrated that these membranes exhibit high flux with the same filtration efficiency, because of the inherent properties of electrospun nanofibres. They have high porosity, interconnected pores and tuneable pore sizes, which can overcome the limitations of conventional TFC membranes [1,2,4].

Despite the good properties and productivity of nanofibrous-based TFC membranes, most of these membranes are usually made from synthetic polymers and contribute to environmental pollution when disposed [2,6]. In this study we demonstrate high flux TFC membranes made of natural polymers, which are chitosan as coating layer and electrospun alginate as mid-layer. Chitosan is a biodegradable polysaccharide polymer derived from the second most available natural polymer on earth, chitin [5,7,8]. Chitin is found on the exoskeleton of crustaceans, crabs and shrimp shells, insects and fungal mycelia [5,8]. It can also be obtained from the wastes of mushrooms such as *Agaricus bisporus*. More than 1000 metric tons/year of chitin is generated from mushroom wastes [5]. Chitosan is generated from the deacetylation of chitin. It is composed of N-acetyl-D-glucosamine and D-glucosamine monomeric units [5,9]. The D-glucosamine content is directly dependent on the degree of chitin deacetylation. A high degree of deacetylation would lead to a large number of positively charged groups on the chitosan backbone, which mainly contribute to its unique properties such as chelation of metal ions and inhibition for the growth of a variety of fungi, yeasts and microorganisms [5,7]. Desai *et al*. [5] fabricated nanofibrous filter media by electrospinning PEO/chitosan blend solutions onto a spunbonded non-woven propylene substrate. They reported a 2-3 log reduction in the *E. coli* cfu with only 6 hours contact time

due to the presence of protonated amine groups. Chitosan has also been used as barrier layer to improve the antifouling and selectivity of the filtration membrane [4,5,10]. Yoon *et al*. [4] prepared a high flux nanofiltration (NF) medium based on electrospun polyacrylonitrile (PAN) coated with chitosan. The membrane exhibited an order of magnitude higher flux rate than a commercial NF filter, while maintaining high filtration efficiency with a rejection ratio greater than 99.9% compared to commercial NF.

Alginate has been selected due to its strong interaction with chitosan *via* complexation. It is a linear polysaccharide copolymer composed of two monomeric units, β-D-mannuronic acid and α-L-guluronic acid [8,11]. It is extracted from brown seaweeds (algae) [11]. Recently, alginate has been studied as a part of the membranes to enhance antifouling [12-14 Zhang *et al*. [12] prepared a freestanding calcium alginate/polyacrylamide hydrogel nanofiltration membrane to evaluate the antifouling and dye rejection of the membrane. The membrane showed good antifouling properties with 89 and 86% water flux recovery for yeast suspension and BSA solutions, and with ~100% rejection of Brilliant Blue G250 (M_w = 854 g mol^{-1}). Similarly, Zhao *et al*. [13] reported that the calcium alginate hydrogel membrane prepared using polyethylene glycol as pore-forming agent rejected ~100% and ~99% of Brilliant Blue G250 and Congo Red, respectively. Although these membranes exhibited good antifouling properties with high selectivity, more research is necessary in the development of the membranes that can exhibit both high flux and selectivity at relatively low operating pressure. For instance, Guo *et al*. [14] prepared a three-tier membrane composed of calcium alginate/carbon nanotubes as selective layer, electrospun polyhydroxybutyrate (PHB)-calcium alginate as midlayer, and PHB nanofibrous substrate to treat a simulated dye (Brilliant Blue) and oily wastewater. The membrane displayed a flux of 36.7 L m^{-2} h^{-1} for pure water and 30.9 L m^{-2} h^{-1} for oil emulsions after 60 minutes of filtration, and the rejection of oil emulsions was 98% due to its hydrophilic nature and good antifouling property. The flux for Brilliant Blue dye was 33.0 L m^{-2} h^{-1} with a rejection rate of 98%.

In this study we attempted to develop a water filtration membrane composed mostly of natural polymers. Three-tier composite membranes composed of alginate nanofibers, electrospun onto a mechanical support layer of non-woven polyethylene terephthalate (PET) fabric as a midlayer, and coated with either chitosan (CaA-CS) or silver nanoparticles containing chitosan (CaA-AgNPs) as selective barrier layer, was fabricated. The silver nanoparticles were synthesized by using chitosan as reducing and capping agent *via* thermal treatment. Dual crosslinking (calcium and glutaraldehyde) was utilized to improve the stability of electrospun alginate nanofibres in water. The membranes were characterized to

evaluate their performance compared to commercial available membranes. This work opens up a new dimension to explore a combination and the use of abundant available natural polymers for filtration applications.

2. Materials and methods

2.1 Materials

Poly(ethylene oxide) (PEO) molecular weight = 1000 kDa; and sodium alginate (SA) from brown algae with guluronic to mannuronic (M/G) ratio of 1.56, viscosity ~250 cP, M_w = 80-120 kDa and dimethylsulphoxide (DMSO, 99%) were purchased from Sigma Aldrich, South Africa. Triton^{TM} X-100 with a density of 1.07 g cm^{-3} and molecular weight of 625 g mol^{-1} was obtained from Sigma Aldrich, South Africa. It is a commercial non-ionic surfactant based on a hydrophilic polyethylene oxide and hydrophobic aromatic hydrocarbon lipophilic, and was used to reduce the surface tension of the blend (PEO and SA) solution to improve its spinnability, and to disperse oil in water for the oil/water separation evaluation. Silver nitrate ($AgNO_3$) 99.8% and acetic acid 99.7% (both from Ibhayi Laboratory Supplies, South Africa); and chitosan (CS) from shrimp shells, deacetylation 75-85%, molecular weight =190-310 kDa (purchased from Sigma Aldrich, South Africa) were used to synthesize silver nanoparticles. $CaCl_2$ 96% and ethanol 99% were purchased from Ibhayi Laboratory Supplies, South Africa and used for leaching the PEO from the nanofibres and crosslinking. Further crosslinking of the nanofibres was established by using HCl (37%) from Ibhayi Laboratory Supplies, South Africa and glutaraldehyde (GA), 25 wt% in water, from Sigma Aldrich, South Africa. Congo Red dye purchased from Fluka Chemical Cooperation, South Africa was used as a model dye to determine the dye removal efficiency of the membranes. The commercial membrane (PLAC07610) (PLA), regenerated and cellulose-based, with a molecular weight cut-off (MWCO) of 1 kDa purchased from Millipore, South Africa was tested for comparison. Polyethylene terephthalate (PET) fabric was used as the substrate for the thin film composite membrane, and it was provided by the Council for Scientific and Industrial Research (CSIR), Port Elizabeth. Silicon dioxide nanoparticles (10-35 nm) obtained from Sigma Aldrich, South Africa was used to investigate the particle rejection capacity of the membranes.

2.2 Fabrication of composite membrane

The PEO/SA nanofibres were prepared by dissolving PEO (3 wt%) and SA (3 wt%) separately in deionized water. A 50/50 v/v mixture of the PEO and SA solutions was stirred for 4 hours and stored in an environmental chamber (Binder GmBH) set at ~25 °C for 10 days. 0.5 wt% Triton X-100 and 5 wt% DMSO were added to the mixture to improve the nanofibrous structure of the resulting fibres. For the electrospinning process, a 20 mL syringe with a stainless steel needle was filled with the blend solution and mounted onto a syringe pump working at a constant flow rate of 0.7 mL h^{-1}. The needle was clamped to the positive electrode of a high voltage supply generating 25 kV, and the grounded electrode was connected to an aluminium collector (tip-to-collector distance was 18 cm). The nanofibres were then ionically crosslinked with calcium chloride by soaking it in 80% ethanol for 5 min and rinsing with a 2 wt% $CaCl_2$ in ethanol solution for 10 min. The nanofibres were incubated in an aqueous solution of $CaCl_2$ for an hour, and then immersed in deionized water for another hour. The $CaCl_2$ treated membranes were then rinsed with deionized water, followed by washing with absolute ethanol, and dried at room temperature.

For filtration analysis, the alginate was electrospun onto a PET nonwoven fabric clamped onto an aluminium collector. The membrane was further crosslinked with glutaraldehyde vapour in a desiccator at room temperature for 24 hours. The pH value of the glutaraldehyde solution was adjusted to 3 using hydrochloric acid, and the glutaraldehyde concentrations were varied from 0.01 M to 0.1 M. The optimal concentration was established by evaluating the swelling behaviour of the crosslinked nanofibres (Figure S1). This test was carried out by immersing the electrospun alginate nanofibre and dual crosslinked nanofibre mats in a bath of distilled water at ambient conditions for 24 hours. The excess water was removed using a filter paper followed by weighing with an analytical balance. The water absorption percentage (*W (%)*) of the membranes was calculated by taking the difference between the final weight and initial weight divided by the initial weight. Finally, the AgNPs containing chitosan solutions were coated onto the nanofibrous membrane. The AgNPs containing chitosan was obtained by mixing 0.07 wt% chitosan and 10 mM silver nitrate, and heating at 90 °C for 12 hours. 2 wt% of chitosan was mixed with 0.07 wt% of AgNPs containing chitosan at 50/50 v/v to increase the viscosity of the solution to control the infusion of the solutions into the mats. A similar procedure was followed in the case of the

non-silver containing chitosan solutions. The membranes' acronyms and descriptions are given in Table 1.

Table 1 Acronyms and their descriptions for the membranes used in this study

Abbreviations	Description
CaA	Ionically crosslinked alginate
Ga-CaA	Glutaraldehyde crosslinked electrospun alginate
CaA-CS	Glutaraldehyde crosslinked electrospun alginate coated with chitosan
CaA-AgNPs	Glutaraldehyde crosslinked electrospun alginate coated with chitosan-containing AgNPs
PLA	Commercial ultrafiltration membrane (PLAC07610)

2.3 Structural characterization

The IR spectra were obtained using a Perkin Elmer Spectrum 100 FTIR spectrometer equipped with an attenuated total reflection (ATR) accessory with a diamond/ZnSe crystal. The spectra were collected after 64 scans over a wavenumber range 500-4000 cm^{-1}, with a resolution 4 cm^{-1}.

The morphology and composition of the electrospun nanofibres and nanofibrous composite materials were examined by a TESCAN VEGA-II scanning electron microscope (SEM) equipped with an energy dispersive X-ray analyser (EDX) for elemental analysis.

The specific area of the composite membranes before and after coating with chitosan solutions were determined using the Brunauer-Emmett-Teller method (BET, Tristar 3000) from nitrogen adsorption measurements. The pore sizes were established from the adsorption isotherms using the Barrett-Joyner-Halenda (BJH) method.

2.4 Antibacterial studies

The antibacterial activity of the nanofibrous composites towards gram negative (*Escherichia coli (ATCC 8739)* and gram positive (*Staphylococcus aureus (ATCC 6538)* bacteria was investigated by an agar well diffusion method. A Mueller-Hinton broth was used at 37 °C for 12-20 hours to revive the bacterial cultures obtained from the Department of Zoology and

Entomology, University of the Free State. The Mueller-Hinton agar medium was prepared and sterilized at 120 °C for 15 minutes. The agar medium was transferred into sterile petri dishes and allowed to solidify under laminar airflow. About 100 μL of the revived bacterial cultures were then cultured on the surface of the medium. The nanofibrous composites (~1 cm × 1 cm) were placed on a glass plate and incubated at 37 °C for 24 h. The inhibition zone formed around the coated nanofibre membrane was measured using a digital calliper and recorded as the antibacterial efficacy.

2.5 Water permeability and nanoparticles separation test

Water permeability was determined using an Amicon® stirred ultrafiltration cell model 8400 which was able to withstand a maximum pressure of 75 psi, with a feed capacity of 400 mL. A circular membrane with a diameter of 76 mm and an effective area of 41.8 cm^2 was fixed into the stirred cell and the water was filtered through the membrane at ambient conditions. The pressure was applied by using nitrogen gas to the feed solution, and the time required to pass equal volumes of solution through the membranes was measured. This test was performed using pressures ranging from 3 to 36 psi.

For the removal of contaminants from water streams, silica nanoparticles were used as model contaminants. 0.05 g of SiO_2 (10-35 nm, determined by BET analysis) were dispersed in 100 mL of water by sonication for 15 minutes and allowed to pass through the membranes using an Amicon® stirred ultrafiltration cell model 8400 at ambient temperature, and the pressure was kept at 3 psi. The transmittance of both the feed and filtrate solutions was measured from 300 to 900 nm with a Shimadzu UV-3100 (190-1100 nm) UV-Vis-NIR recording spectrophotometer at a resolution of 0.5 nm. The concentrations of the mixtures were determined through UV-vis spectroscopy.

2.6 Oil/water separation

To evaluate the oil/water separation ability of the membrane systems, oily wastewater was prepared by mixing vegetable oil with distilled water and Triton X-100 surfactant for 20 minutes using a homogenizer at 5000 rpm. The oil to water ratio was 1:20. A circular membrane fixed into an Amicon® ultrafiltration stirred cell and 20 mL of the oil solution was filtered through the membrane at ambient conditions and a pressure of 3 psi. The

transmittance of both the feed and permeates was measured with a Shimadzu UV-3100 (190-1100 nm) UV-Vis-NIR recording spectrophotometer.

2.7 Dye removal

For the evaluation of the dye removal efficiency of the membranes, Congo Red (CR) was used as a model dye. The filtration process was carried out by filtering 50 mL of CR solution through the membrane at ambient conditions and a pressure of 0.3 psi. The filtration process was repeated 5 times and the membrane was flushed with pure water after each filtration cycle. The concentration of the dye was then measured with a Shimadzu UV-3100 (190-1100 nm) UV-Vis-NIR recording spectrophotometer. The amount of dye removed was calculated from the concentration change before and after filtration, as determined by optical absorption at 498 nm.

3. Results and discussion

3.1 Electrospun alginate nanofibers

To find the optimum concentration of glutaraldehyde, the swelling properties of the chemically crosslinked fibres were studied by immersion in water for 24 hours to find the optimum glutaraldehyde concentration for crosslinking the alginate fibres (Figure S1). It was found that the chemical crosslinking reduced the swelling of the fibres from ~160% to less than 50% using 0.1 M of glutaraldehyde for 24 hours. Concentrations higher than 0.1 M led to considerable shrinkage and a colour change of the mats to yellowish (Figure S2). Thus, fibres treated with 0.1 M glutaraldehyde for 24 hours were used throughout the study. The SEM images of the electrospun nanofibre membranes of the PEO/sodium alginate blend (PEO/SA), as well as calcium crosslinked (CaA) and dual crosslinked (calcium and glutaraldehyde crosslinked (GA-CaA)) alginate nanofibers, are shown in Figure 1. In the case of the PEO/SA blends solution, well defined nanofibres without any structural defects were obtained (Figure 1(a)). The mean diameter of the fibres was approximately 97.4 ± 20.3 nm. After the ionic crosslinking using calcium chloride (CaA), the fibres interfused into an interlocked network structure (Figure 1(b)). Some of these fibres adhered to each other at different bonding sites to form a film-like structural integrity, while the fibres maintained their nanofibrous structure.

However, the average diameter of the fibres slightly increased to 144 ± 48 nm, which could be due to the swelling of the fibres during dissolution of PEO. The dual crosslinking (Ga-CaA) led to a more significant binding of the fibres and the diameter (152 ± 45 nm) of the fibres was not significantly influenced compared to that of the ionically crosslinked fibres (Figure 1(c)).

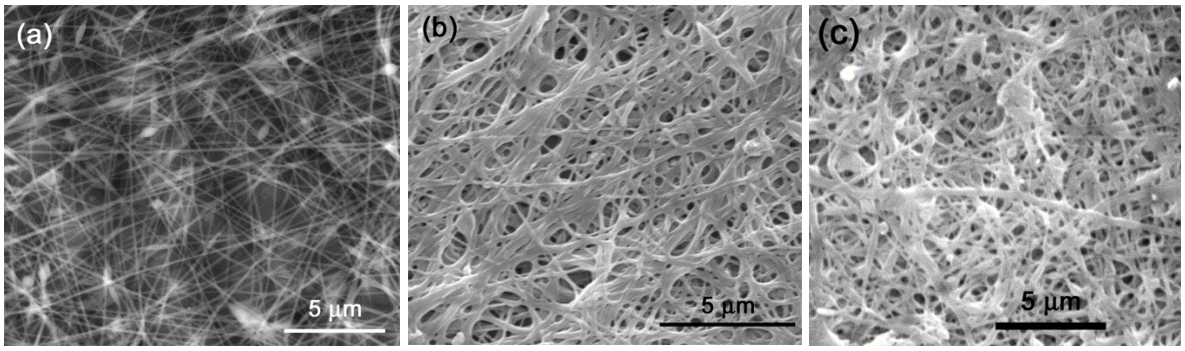

Figure 1 SEM images of (a) PEO/SA, (b) ionically crosslinked alginate (CaA), and (c) glutaraldehyde crosslinked nanofibres (Ga-CaA)

The IR spectra for the different electrospun nanofibre membranes are shown in Figure 2. The CaA nanofibres displayed absorption bands at 3268, 1589, 1414, and 1026 cm^{-1} corresponding to –OH stretching, COO^- asymmetric stretching, COO^- symmetric stretching and C-O-C stretching, respectively. All these vibrations correspond to those of the pure alginate [8,15]. The electrospun PEO/SA blend fibres showed similar peaks to those of the CaA nanofibers, with additional peaks at 2881 cm^{-1} (CH stretching), 1456 cm^{-1} (CH_2 wagging), 1100 and 839 cm^{-1} (C-O-C stretching and bending), and 960 cm^{-1} corresponding to CH_2 rocking and twisting. These peaks are related to the presence of PEO, and they disappeared after ionic crosslinking because of the washing of the fibres in water during which the PEO was removed through dissolution. After chemical crosslinking with glutaraldehyde, the -OH stretching peak at 3268 cm^{-1} shifted to 3338 cm^{-1} because the -OH groups would have taken part in the formation of acetyl bridges between the alcohol groups in the alginate and the aldehydes in glutaraldehyde [16,17]. Leung *et al*. [17] observed a similar shift in the -OH stretching after crosslinking with glutaraldehyde because of the reaction between the alginate and glutaraldehyde. The new absorption peaks at 1345 cm^{-1}, 839 cm^{-1} and 959 cm^{-1} correspond to the C-O-C vibrations from the acetyl rings and ether linkages. The presence of these peaks, the shift in the -OH peak, and the presence of a new peak at 1345 cm^{-1} confirmed the crosslinking of the alginate with glutaraldehyde through the formation of acetyl and ethyl linkages [16]. The absorption bands at 2860 (C-H stretching) and 1606 cm^{-1}

(C=O stretching) became more resolved are ascribed to the aldehyde groups [17]. In the crosslinking of the alginate with glutaraldehyde, only one aldehyde group is often used for two carboxyl groups from the alginate [16]. Therefore, the increase in intensity and sharpening of these absorption bands is probably due to the unreacted aldehydes on the surfaces of the alginate polymer chains. This is confirmed by an increase in the intensity of these peaks with an increase in concentration (see Figure S3 in the supporting material).

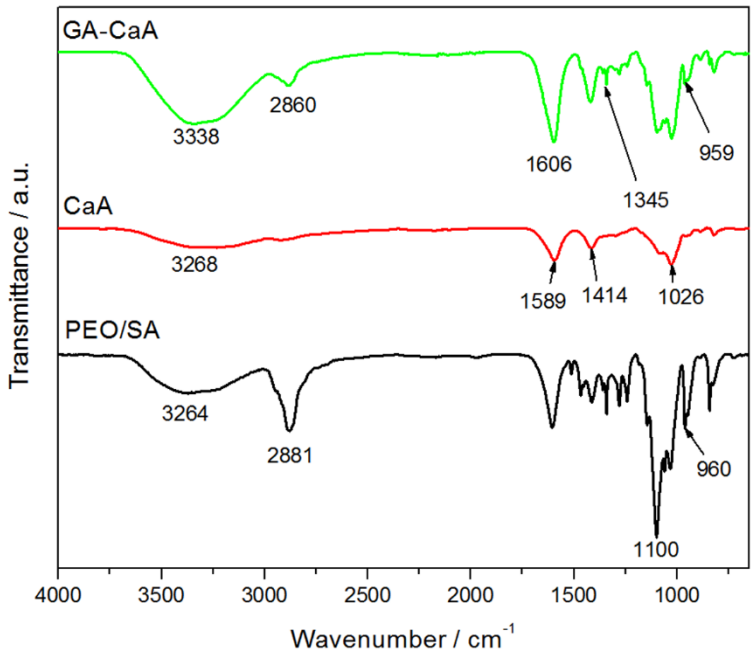

Figure 2 FTIR spectra of uncrosslinked and crosslinked alginate nanofibres

3.2 Nanofibrous composite membrane

Figure 3 shows the surface morphology of CaA-CS and CaA-AgNPs. The chitosan coated membrane shows a smooth and flat surface (Figure 3(a)), while in the chitosan/AgNPs coated membrane the layer was rough with white spots well dispersed throughout the picture (Figure 3(b)). These spots can be attributed to the silver nanoparticles, since they can scatter electrons more than the polymer.

The presence of the silver nanoparticles was confirmed by EDX as shown in Figure 3(c). There is a strong signal for silver at approximately 2.7 keV. This is the result of the surface plasmon of silver which confirms the reduction of the silver ions to elemental silver. Guzman *et al*. [18] and Kaviya *et al*. [19] reported emission peaks for silver nanoparticles at approximately 3 keV. There are also signals for other elements such as oxygen, sodium, and potassium. The presence of oxygen is probably from chitosan. Sodium and potassium were

contaminants in the silver nitrate, that were mentioned in the manufacturer' specification sheet.

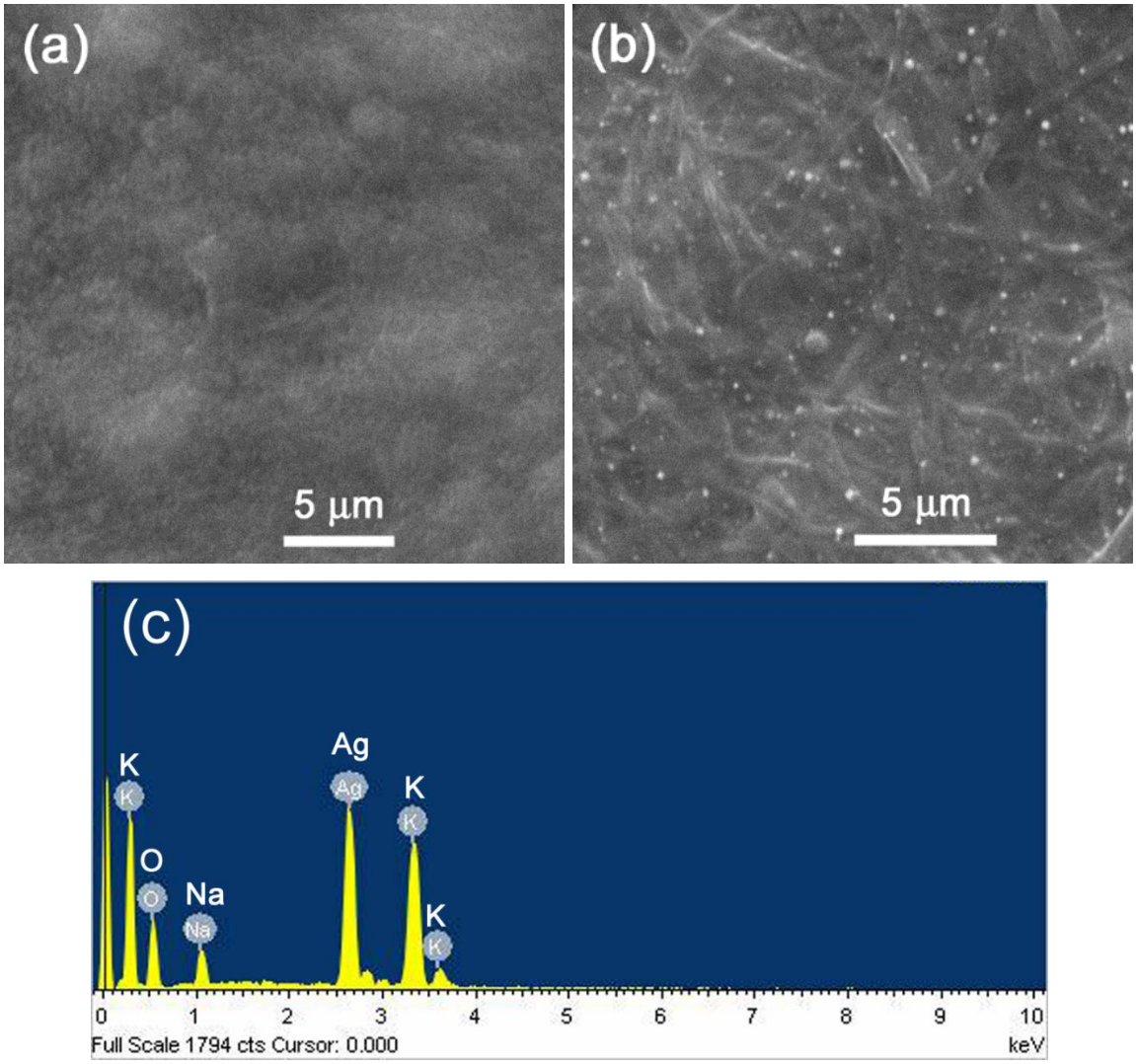

Figure 3 SEM micrographs of (a) CaA-CS, (b) CaA-AgNPs and (c) EDX spectra of CaA-AgNPs

3.3 Antibacterial studies

The antibacterial efficiency of the composite membranes was evaluated by the zone inhibition method (Figure 4 and results tabulated in Table 2). Glutaraldehyde crosslinked electrospun alginate nanofibres were used as a control, and no inhibition zone against all strains was observed around its mats (area 1 in Figures 4(a) and 4(b)). The CaA-CS membrane showed a bacteriostatic effect towards *E. coli* (area 2 in Figure 4(a)). This is due to the positive charges on the surface of chitosan which can easily react with negatively charged bacteria and inhibit

the bacterial growth on the mat compared to positively charged bacteria [9]. The CaA-AgNPs membrane showed a high potent towards both *E. coli* and *S. aureus* (area 3 in Figures 4(a) and 4b)). This is due to the presence of the silver nanoparticles. The *E. coli* showed more susceptibility than the *S. aureus*, probably because of the synergistic effect between the chitosan and silver nanoparticles acting towards the gram negative bacteria. The *S. aureus* has a thicker peptidoglycan in the cell wall than the *E. coli*, which acts against the invasion of the AgNPs [20,21]. Silver nanoparticles are well-known for their high potent towards gram negative and gram positive bacteria [21]. However, the exact mechanism of their antibacterial activity is not fully understood and three mechanisms were proposed [18,20,22]. Firstly, the silver nanoparticles (AgNPs) attach to the cell membrane and disturb permeability and respiration. Secondly, AgNPs can penetrate the bacteria and interact with the sulphur and phosphorus containing compounds such as DNA, hence affecting the cell viability. Thirdly, AgNPs release silver ions which contribute to its antibacterial effect [20]. The results demonstrate that the AgNPs coated membrane can eradicate both gram negative and gram positive bacteria, therefore it can be used for anti-biofouling in filtration applications.

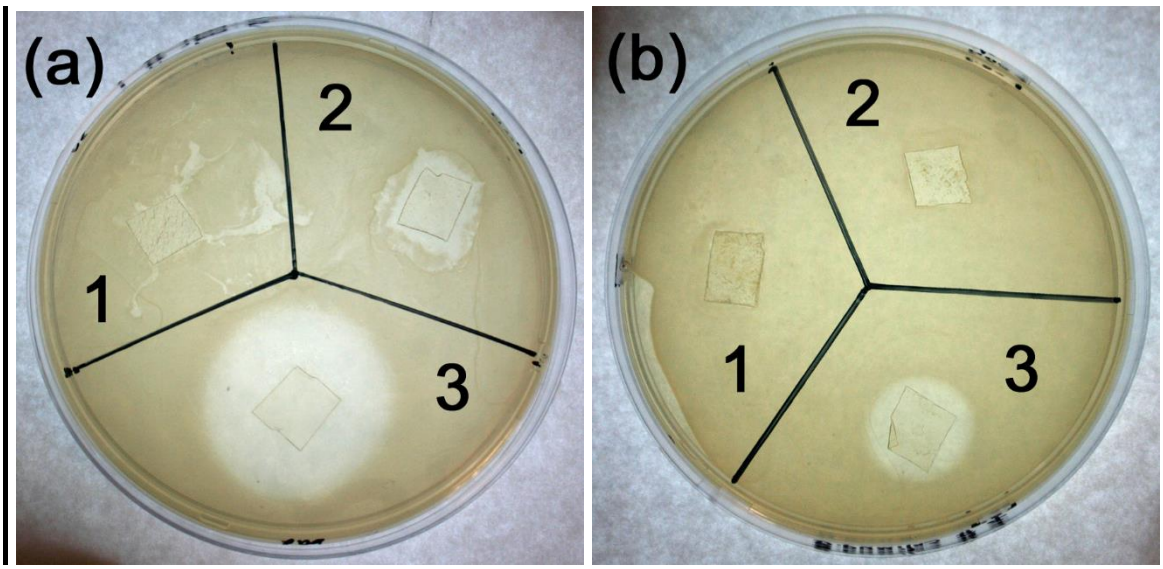

Figure 4 Antibacterial inhibition zones against (a) E. coli and (b) S. aureus. The numbers on the photos indicate Ga-CaA (1), CaA-CS (2), and CaA-AgNPs (3).

Table 2 Comparison of the inhibition zones towards gram negative and gram positive bacteria

Bacteria	**Inhibition zone /cm**		
	Ga-CaA (Zone 1)	**CaA-CS (Zone 2)**	**CaA-AgNPs (Zone 3)**
E. coli	0	0_b	3.32 ± 0.20
S. aureus	0	0	2.31 ± 0.17

b = bacteriostatic

3.4 Water flux and nanoparticle separation efficiency

The pure water flux through the composite membranes is shown in Figure 5. All the tested membranes showed an increase with an increase in pressure, except for the commercial PLA membrane where the flux remained fairly constant independent of the applied pressure. This can be ascribed to the low surface porosity and broad pore size distribution [4]. These properties are often exhibited by membranes that are mainly produced by phase immersion. The effect of coating with chitosan (CaA-CS) and chitosan-containing AgNPs (CaA-AgNPs) can be seen from the difference in flux compared to that of the uncoated dual crosslinked membrane (GA-CaA). The superiority displayed by the uncoated GA-CaA membrane throughout the applied pressure can be attributed to the porous structure of the electrospun nanofibres which formed an interconnected network structure (see Figure 1(c)) resulting in a high filtration flux. CaA-CS, CaA-AgNPs and commercial PLA displayed similar flux, especially at low pressures. At high pressures, there was a clear difference between these membranes. The CaA-CS membrane shows a slightly higher flux than the CaA-AgNPs membrane, which is probably due to the presence of the AgNPs in the selective barrier which reduced the pore size of the membrane. In the case of CaA-CS and CaA-AgNPs, the nanofibres (with high bulk porosity) allowed chitosan to form a thin layer (which may occur due to strong electrostatic interaction between the alginate and chitosan) on top of the membrane surface, which improved the water flux compared to that of the asymmetrical commercial UF membrane (PLA) with low surface porosity (10-20%) and small pore size.

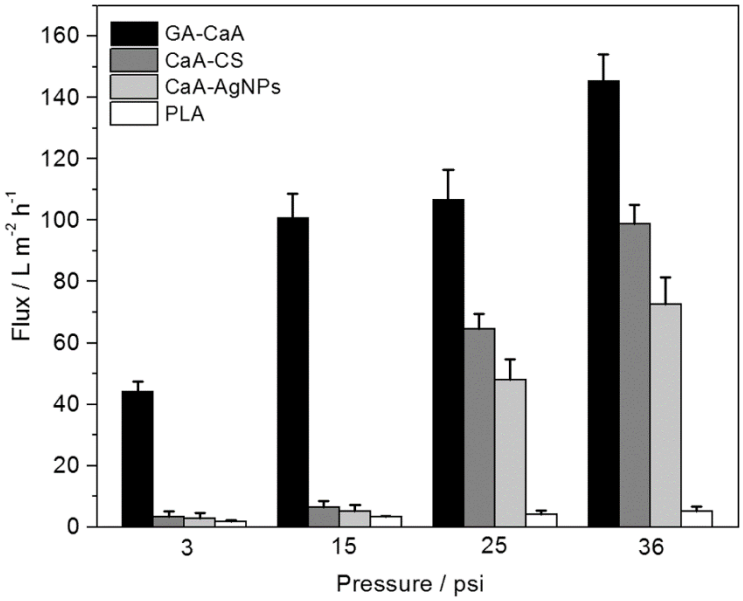

Figure 5 Water permeation of GA-CaA, CaA-CS, and CaA-AgNPs composite membranes

The BET and nanoparticles removal results are summarized in Table 3. Both the specific surface area and the pore size of the GA-CaA membrane decreased after coating with either chitosan or AgNPs containing chitosan. It is clear that the coatings decreased the pore size and surface area, which is probably due to the formation of a thin film/layer on top of the electrospun nanofibres, resulting in smaller pores. This confirms the water permeation results, where the coated membranes showed lower water flux than the GA-CaA membrane.

Table 3 BET results of the membranes nanofibrous composite membranes

Type	BET surface area / $m^2 g^{-1}$	Average pore size / nm	Rejection of 10-35 nm particles / %
GA-CaA	8.06	199	79.1 ± 0.9
CaA-CS	3.08	50.2	98.3 ± 1.5
CaA-AgNPs	2.32	37.6	99.5 ± 0.4
Commercial PLA	-	-	99.6 ± 0.4

The evaluation of the separation capacity and confirmation of the membrane pore size were carried out by filtering SiO_2 (10-35 nm) nanoparticles as model contaminants (Figure 6). The UV spectra of the permeates from both the CaA-CS and CaA-AgNPs membranes were relatively similar to that of pure water. Visually the permeates were more transparent than the feed solution (Figure S4). The filtrates for GA-CaA, on the other hand, showed slightly

different UV spectra for all the tested samples. The Ga-CaA has a high surface porosity with large surface pores that allowed the nanoparticles to pass through the membrane (Figure 1c). However, in the case of the coated membranes (CaA-CS and CaA-AgNPs) the thin layer with smaller pore sizes improved the retention of the nanoparticles (Figure 3a,b). These results confirmed the higher flux displayed by the GaA membrane, with its more porous structure, compared to the coated membranes, with their smaller pore sizes, and PLA (Figure 5). The recorded absorbance at 320 nm was used to confirm the filtration capacity of the membranes (Table 3). For commercial PLA, as well as the CaA-CS and CaA-AgNPs membranes, the particle rejection was greater than 98%, which was probably due to their smaller pore sizes, while for the GA-CaA membrane it was approximately 79%. However, the average pore size of the membranes was bigger than the sizes of the nanoparticles. In this case, the nanoparticles probably entered the mesoporous thin layer on the surface of the membranes and were attracted to the surfaces of the inner pores as they passed through the membrane. This reduced the pore sizes and contributed to the high rejection. The nanoparticles could also have been attracted to the outer surfaces of the membranes, forming a dense 'cake-like' film which contributed to the separation efficiency of the membranes [23,24]. It was visually observed at the end of the filtration test that the membrane surface was covered by a thin layer of the nanoparticles. Wang *et al*. [24] also found that a membrane having a maximum pore size of 0.62 ± 0.03 µm was capable of retaining 93% of particles having a size of 0.20 µm. The particles closely packed together on the surface of the membrane and formed a 'cake layer' on the surface of the membrane, blocking the open active pores and rejecting the particles from passing through the membrane, which led to a high retention ratio.

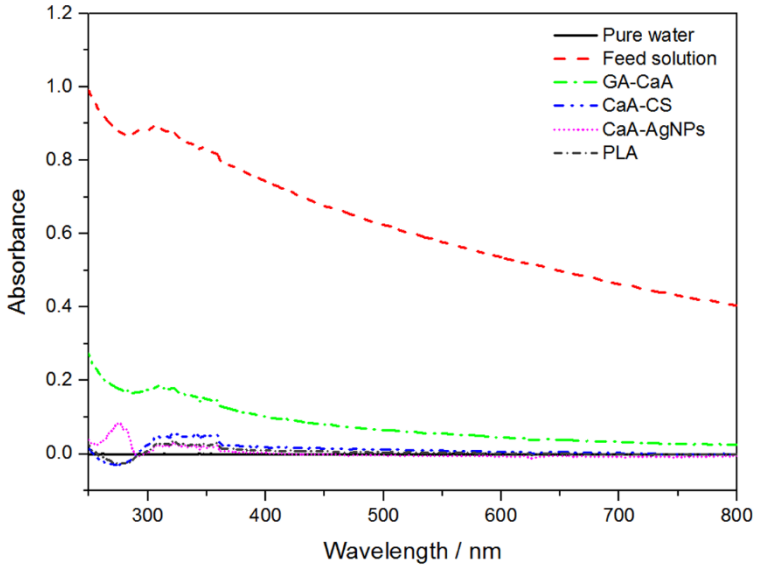

Figure 6 Filtration performance for the TFC membranes to silicon dioxide (SiO_2) rejection at 3 psi

3.5 Oil/water emulsion separation efficiency

Separation of oil/water emulsions was evaluated for the TFC membranes as shown in Figure 7. The UV spectra of the filtrate for the CaA-AgNPs, CaA-CS and commercial PLA membranes are very similar, showing that an acceptable amount of oil was rejected. The Ga-CaA spectrum showed that almost no oil was rejected, which may be ascribed to the large pore size of the porous GA-CaA membrane. The recorded absorbance at 280 nm was used to verify the oil separation efficiency of the membranes (Table 4). The CaA-CS and CaA-AgNPs membranes showed the highest removal efficiency, closely followed by the commercial PLA membrane. The rejection percentage for the Ga-CaA membrane was significantly lower than those of the others. Although the rejection of oil by the membranes may have been due to their hydrophilic character, the smaller pore size of the coated membranes significantly contributed to their more effective oil rejection. The coated chitosan and chitosan containing AgNPs formed a compact structure on top of the electrospun nanofibers (Figure 3a,b), reducing the surface porosity and the sizes of the surface active pores of the membrane, which in turn contributed to the rejection of the oil in the emulsions. However, the Ga-CaA membrane had a large open porous structure (high surface porosity, Figure 1c), which allowed more oil droplets to pass through. This also explains the lower water permeation flux exhibited by the coated membranes and the commercial PLA compared to the porous GaA (Figure 5). The presence of the silver nanoparticles into the chitosan coating layer obviously had no additional influence on the separation behaviour of the membrane, which was to be expected. The visual observations of the solutions are shown in Figure S4.

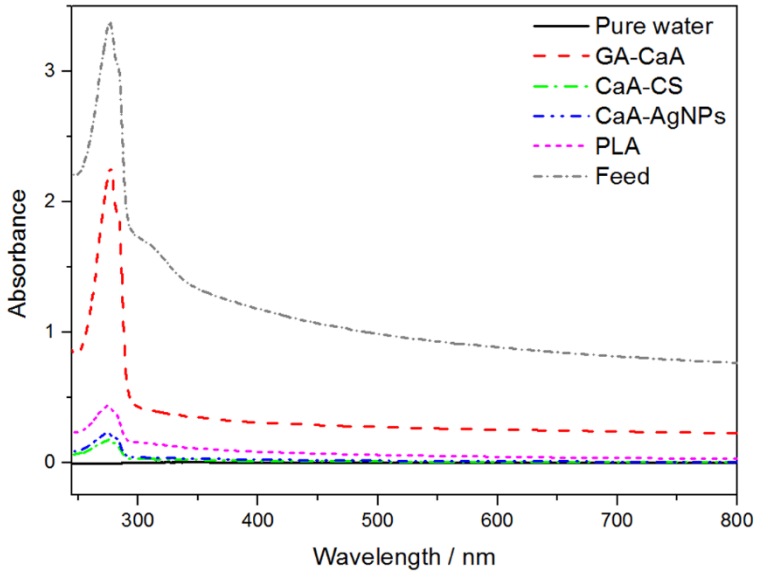

Figure 7 UV-visible spectra of oil concentration after passing through TFC membranes

Table 4 Oil/water emulsion separation efficiency by TFC membranes

Sample	% Rejection
Ga-CaA	33.0 ± 8.9
CaA-CS	94.9 ± 2.0
CaA-AgNPs	93.5 ± 2.6
PLA	87.3 ± 1.0

3.6 Dye removal test

The dye removal efficiency of the TFC membranes was evaluated by passing the CR dye through all the investigated membranes, and the UV spectra of the respective filtrates are shown in Figure 8. The intensity of the peak at 498 nm increased with the number of filtration cycles for both GA-CaA and CaA-CS. For the porous GA-CaA the high rejection during the first filtration cycle was the result of the adsorption of the dye by the membrane due to its large surface area. The adsorption could have been the result of the ionic interaction between the carboxyl groups on the surface of the fibres and the amino groups in the CR dye. However, the membrane performance decreased with an increase in the number of filtration cycles (Figure 9). The reason for this is probably that the dye was initially adsorbed onto the fibre surfaces, but after all the active binding sites were occupied, the remainder of the dye penetrated through the pores of the membrane. The performance of the CaA-CS also

decreased with an increase in the number of filtration cycles. The CaA-AgNPs membrane, however, maintained a fairly high rejection until the third cycle, after which it slightly decreased, while the commercial PLA maintained a high rejection throughout the test. The CaA-CS and CaA-AgNPs membranes have similar functional groups, and therefore the difference between these membranes' performance depended more on the sizes of the pores and on the presence of the silver nanoparticles. It is possible that during the filtration, the crosslinked alginate nanofibres (midlayer) swelled to a certain extent (Figure S1). If this is the case, the surface coating layer may have been damaged, allowing the dye to pass more freely. The presence of the AgNPs in the barrier layer, however, reinforced the coated layer and delayed its damage during the washing and filtration cycles. Even though the CaA-CS and CaA-AgNPs membranes were not yet fully optimized, they displayed comparable rejection percentages to the commercial membrane in the first 2 to 3 filtration cycles. These results are in line with the differences in water permeation flux between the membranes with smaller pore size (coated membranes and PLA) and the porous GaA (Figure 5). The compact structure of the coated membrane and the asymmetrical structure of PLA played the major role in the removal of the dye by these membranes. Crosslinking of the barrier layer could improve its stability, as well as the overall strength performance of these membranes.

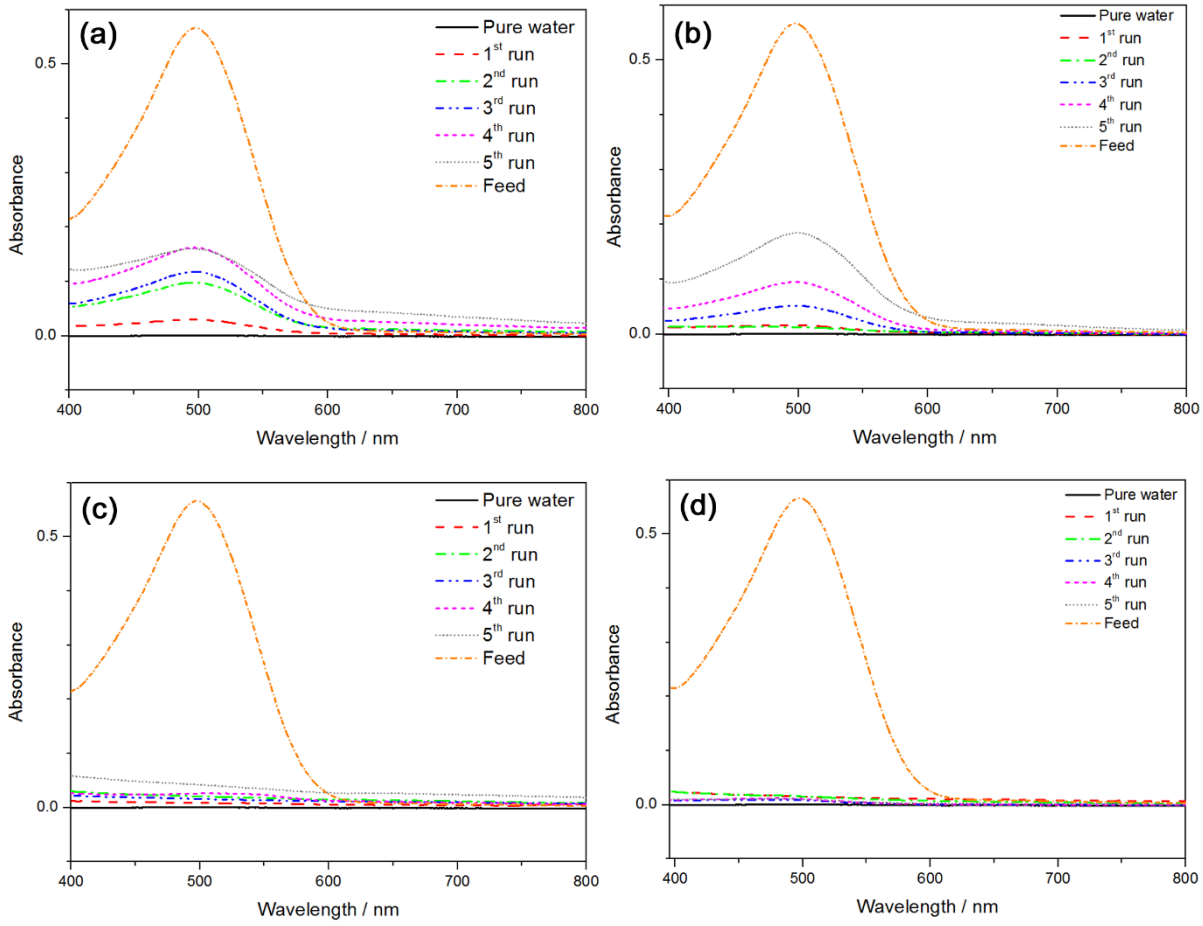

Figure 8 UV-visible spectra of dye after passing through membrane (a) GA-CaA, (b) CaA-CS, (c) CaA-AgNPs, and (d) PLA at 0.3 psi for 5 times

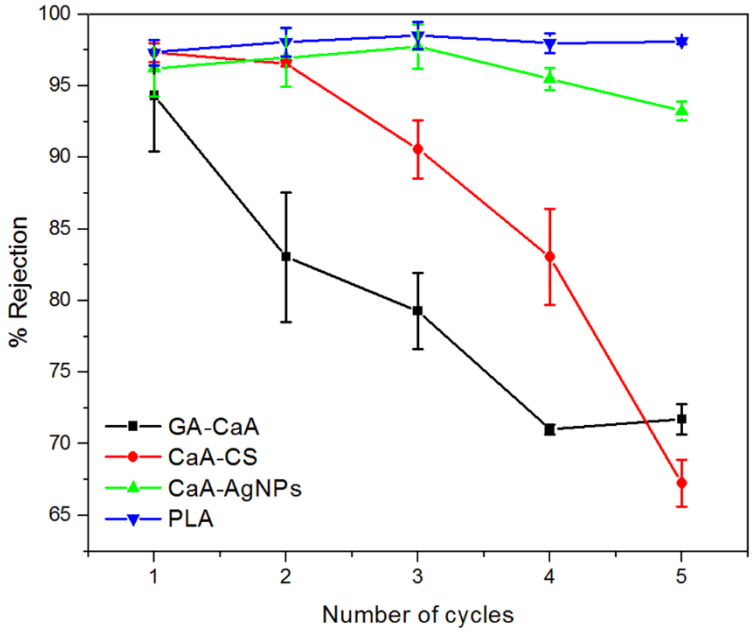

Figure 9 The dye rejection percentage of the composite membranes

Conclusions

A TFC membrane coated with chitosan and silver nanoparticles for water purification was developed. The AgNPs were well dispersed on the surface of the membrane and showed good antibacterial activity against both gram negative and gram positive bacteria. The presented results suggest that the presence of AgNPs in the selective barrier layer can improve the stability and the antibacterial activity of the membrane without affecting the membrane productivity. Both the chitosan and chitosan-containing coated membranes exhibited a higher flux than the commercially available membrane (PLAC07610), while maintaining a good rejection of the nanoparticles (10-35 nm) and oil emulsions. The nanoparticle retention was greater than 98%, while the oil removal was greater than 93%. The chitosan containing AgNPs membrane displayed superior dye rejection than the chitosan coated membrane over all the tested filtration cycles (with dye rejection above 95%). The CaA-AgNPs also displayed a comparable dye rejection (> 98%) for the first three filtration cycles to the commercial available membrane (PLA) due to reinforcement of the coated layer by the silver nanoparticles. It can therefore be concluded that the simple synthesis of AgNPs using chitosan, and the low cost of chitosan and alginate, can provide a membrane like the CaA-

AgNPs membrane which can be used to resist the adhesion of micro-organisms without hampering the membrane productivity. This provides a promising potential application for oil and dye separation. Work in progress currently focusses on the crosslinking of the barrier layer to improve the stability under applied pressures during filtration.

Acknowledgements

The authors would like to thank the Department of Science and Technology-National Research Foundation of South Africa (DST-NRF), Professional Development Programme for their financial support.

References

[1] S. Subramanian, R. Seeram, New directions in nanofiltration applications – Are nanofibers the right materials as membranes in desalination?, Desalination, 308 (2013) 198-208.

[2] H. Ma, C. Burger, B.S. Hsiao, B. Chu, Ultrafine polysaccharide nanofibrous membranes for water purification, Biomacromolecules, 12 (2011) 970-976.

[3] S.-J. Park, R.K. Cheedrala, M.S. Diallo, C. Kim, I.S. Kim, W.A. Goddard III, Nanofiltration membranes based on polyvinylidene fluoride nanofibrous scaffolds and crosslinked polyethyleneimine networks, Journal of Nanoparticle Research, 14 (2012) 1-14.

[4] K. Yoon, K. Kim, X. Wang, D. Fang, B.S. Hsiao, B. Chu, High flux ultrafiltration membranes based on electrospun nanofibrous PAN scaffolds and chitosan coating, Polymer, 47 (2006) 2434-2441.

[5] K. Desai, K. Kit, J. Li, P. Michael Davidson, S. Zivanovic, H. Meyer, Nanofibrous chitosan non-wovens for filtration applications, Polymer, 50 (2009) 3661-3669.

[6] X. Wang, D. Fang, K. Yoon, B.S. Hsiao, B. Chu, High performance ultrafiltration composite membranes based on poly(vinyl alcohol) hydrogel coating on crosslinked nanofibrous poly(vinyl alcohol) scaffold, Journal of Membrane Science, 278 (2006) 261-268.

[7] K. Sun, Z. Li, Preparations, properties and applications of chitosan based nanofibers fabricated by electrospinning, eXPRESS Polymer Letters, 5 (2011) 342-361.

[8] S.I. Jeong, M.D. Krebs, C.A. Bonino, J.E. Samorezov, S.A. Khan, E. Alsberg, Electrospun chitosan–alginate nanofibers with in situ polyelectrolyte complexation for use as tissue engineering scaffolds, Tissue Engineering Part A, 17 (2010) 59-70.

[9] Y.-C. Chung, H.-L. Wang, Y.-M. Chen, S.-L. Li, Effect of abiotic factors on the antibacterial activity of chitosan against waterborne pathogens, Bioresource Technology, 88 (2003) 179-184.

[10] Z. Zhao, J. Zheng, M. Wang, H. Zhang, C.C. Han, High performance ultrafiltration membrane based on modified chitosan coating and electrospun nanofibrous PVDF scaffolds, Journal of Membrane Science, 394 (2012) 209-217.

[11] J.-W. Lu, Y.-L. Zhu, Z.-X. Guo, P. Hu, J. Yu, Electrospinning of sodium alginate with poly(ethylene oxide), Polymer, 47 (2006) 8026-8031.

[12] X. Zhang, B. Lin, K. Zhao, J. Wei, J. Guo, W. Cui, S. Jiang, D. Liu, J. Li, A free-standing calcium alginate/polyacrylamide hydrogel nanofiltration membrane with high anti-fouling performance: Preparation and characterization, Desalination, 365 (2015) 234-241.

[13] K. Zhao, X. Zhang, J. Wei, J. Li, X. Zhou, D. Liu, Z. Liu, J. Li, Calcium alginate hydrogel filtration membrane with excellent anti-fouling property and controlled separation performance, Journal of Membrane Science, 492 (2015) 536-546.

[14] J. Guo, Q. Zhang, Z. Cai, K. Zhao, Preparation and dye filtration property of electrospun polyhydroxybutyrate-calcium alginate/carbon nanotubes composite nanofibrous filtration membrane, Separation and Purification Technology, 161 (2016) 69-79.

[15] N. Bhattarai, M. Zhang, Controlled synthesis and structural stability of alginate-based nanofibers, Nanotechnology, 18 (2007) 455601.

[16] C. Yeom, K.H. Lee, Characterization of sodium alginate membrane crosslinked with glutaraldehyde in pervaporation separation, Journal of Applied Polymer Science, 67 (1998) 209-219.

[17] V. Leung, R. Hartwell, S.S. Elizei, H. Yang, A. Ghahary, F. Ko, Post electrospinning modifications for alginate nanofiber-based wound dressings, Journal of Biomedical Materials Research Part B: Applied Biomaterials, 102 (2014) 508-515.

[18] M. Guzman, J. Dille, S. Godet, Synthesis and antibacterial activity of silver nanoparticles against gram-positive and gram-negative bacteria, Nanomedicine: Nanotechnology, Biology and Medicine, 8 (2012) 37-45.

[19] S. Kaviya, J. Santhanalakshmi, B. Viswanathan, J. Muthumary, K. Srinivasan, Biosynthesis of silver nanoparticles using Citrus sinensis peel extract and its antibacterial activity, Spectrochimica Acta Part A: Molecular and Biomolecular Spectroscopy, 79 (2011) 594-598.

[20] Q. Feng, J. Wu, G. Chen, F. Cui, T. Kim, J. Kim, A mechanistic study of the antibacterial effect of silver ions on Escherichia coli and Staphylococcus aureus, Journal of Biomedical Materials Research, 52 (2000) 662-668.

[21] T. Maneerung, S. Tokura, R. Rujiravanit, Impregnation of silver nanoparticles into bacterial cellulose for antimicrobial wound dressing, Carbohydrate Polymers, 72 (2008) 43-51.

[22] M. Rai, A. Yadav, A. Gade, Silver nanoparticles as a new generation of antimicrobials, Biotechnology Advances, 27 (2009) 76-83.

[23] R. Gopal, S. Kaur, Z. Ma, C. Chan, S. Ramakrishna, T. Matsuura, Electrospun nanofibrous filtration membrane, Journal of Membrane Science, 281 (2006) 581-586.

[24] R. Wang, Y. Lui, B. Li, B.S. Hsioa, B. Chu, Electrospun nanofibrous membranes for high flux microfitration, Journal of Membrane Science, 392-393 (2012) 167-174.

Supporting material

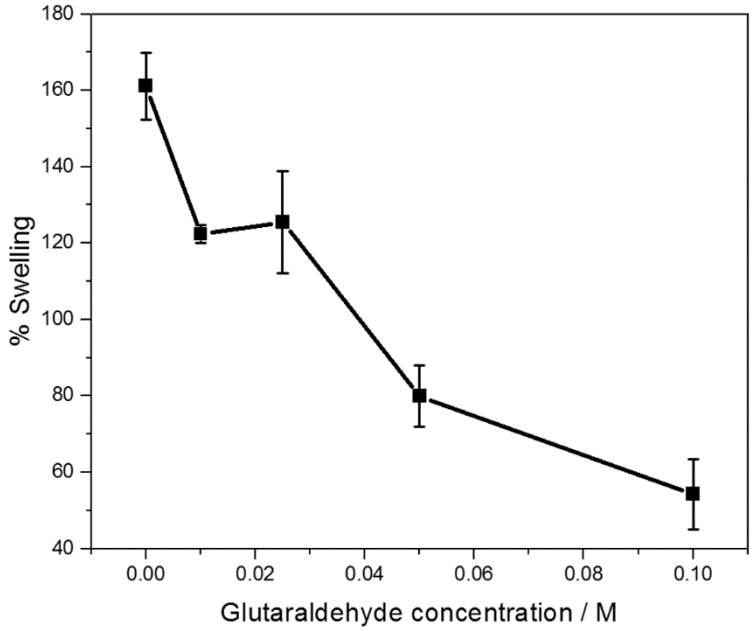

Figure S1 Swelling behaviour of crosslinked alginate nanofibres versus glutaraldehyde concentration

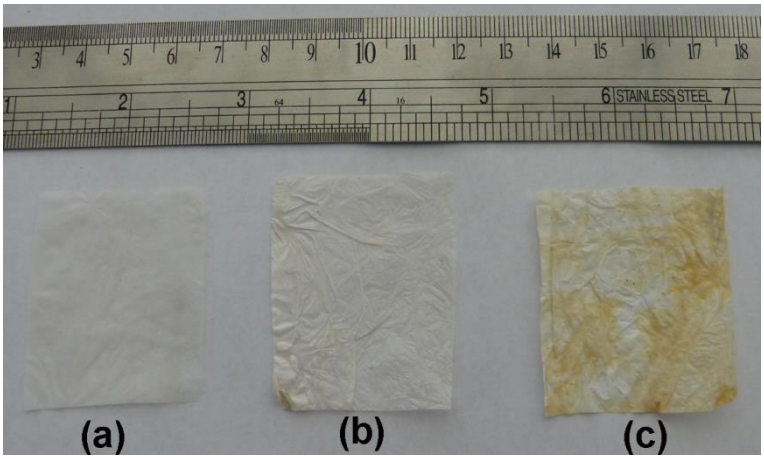

Figure S2 Images of electrospun nanofibres: (a) uncrosslinked, and crosslinked with (b) 0.1 M and (c) 0.2M glutaraldehyde for 24 hours

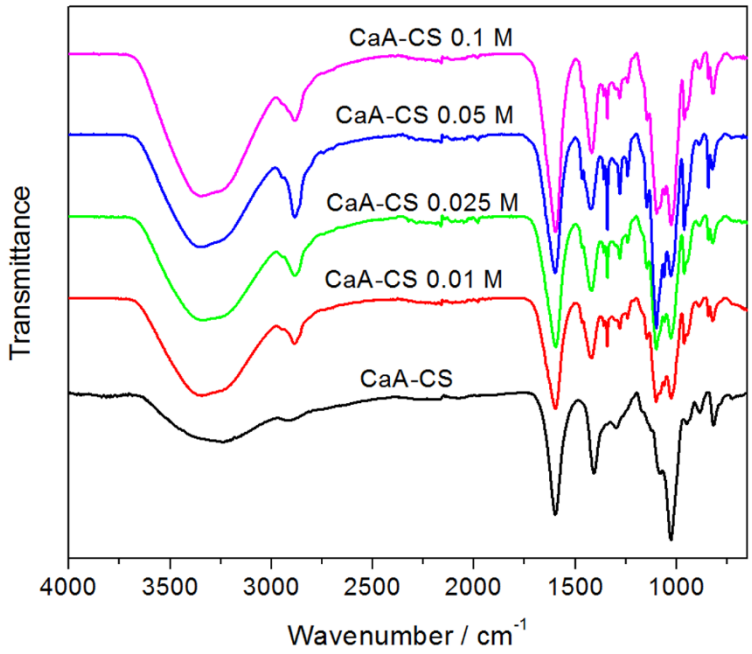

Figure S3 FTIR spectra of alginate crosslinked with different glutaraldehyde concentrations for 24 hours

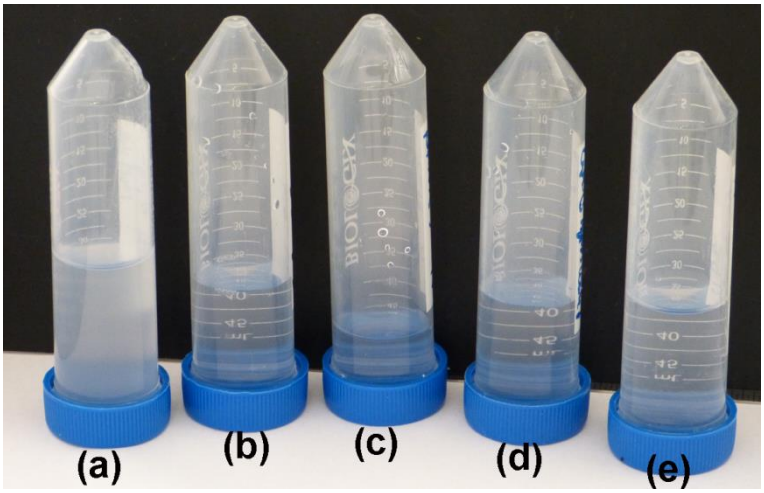

Figure S4 The permeates from SiO_2 filtration with TFC membranes: (a) feed, (b) GA-CaA, (c) CaA-CS, (d) CaA-AgNPs, and (e) PLA

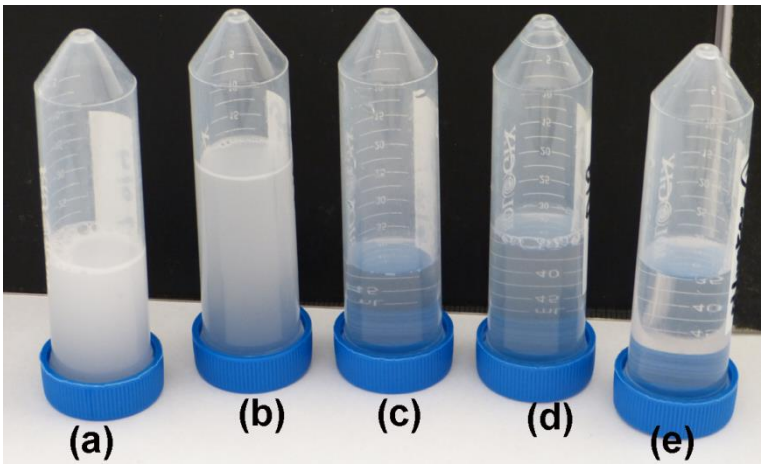

Figure S5 The filtrates from oil separation for TFC membranes: (a) feed, (b) GA-CaA, (c) CaA-CS, (d) CaA-AgNPs, and (e) PLA